THE UNIVERSITY of EDINBURGH

Edinburgh Research Explorer

Hybrid Polystyrene Nanoparticle-Ultrafiltration System for Hormone Removal from Water

Citation for published version:
Akanyeti, I, Kraft, A & Ferrari, M-C 2017, 'Hybrid Polystyrene Nanoparticle-Ultrafiltration System for Hormone Removal from Water', *Journal of Water Process Engineering*.
https://doi.org/10.1016/j.jwpe.2017.02.014

Digital Object Identifier (DOI):
10.1016/j.jwpe.2017.02.014

Link:
Link to publication record in Edinburgh Research Explorer

Document Version:
Peer reviewed version

Published In:
Journal of Water Process Engineering

General rights
Copyright for the publications made accessible via the Edinburgh Research Explorer is retained by the author(s) and / or other copyright owners and it is a condition of accessing these publications that users recognise and abide by the legal requirements associated with these rights.

Take down policy
The University of Edinburgh has made every reasonable effort to ensure that Edinburgh Research Explorer content complies with UK legislation. If you believe that the public display of this file breaches copyright please contact openaccess@ed.ac.uk providing details, and we will remove access to the work immediately and investigate your claim.

Download date: 08. May. 2023

Hybrid Polystyrene Nanoparticle-Ultrafiltration System for Hormone Removal from Water

İme Akanyeti[a,b] *, Arno Kraft*[c] *and Maria-Chiara Ferrari*[a]*‡

[a] School of Engineering, University of Edinburgh, Robert Stevenson Road, Edinburgh EH9 3FB, UK

[b] Department of Environmental Engineering, Faculty of Engineering, Cyprus International University, Haspolat, Lefkoşa, North Cyprus, Mersin 10 Turkey

[c] Institute of Chemical Sciences, School of Engineering and Physical Sciences, Heriot-Watt University, Edinburgh, EH14 4AS, UK

ABSTRACT

Occurrence of hormones in water resources even at low concentrations of ng/L is a potential risk for both environmental and public health. Hybrid sorbent-ultrafiltration (UF) systems are among the technologies under investigation for their potential as a sustainable and energy-efficient process for the removal of hormones from water. In this study polystyrene (PS) nanoparticles were explored as sorbent in a hybrid system. Estrone adsorption capacity of 52 nm PS nanoparticles was found to be 79.6 ng/g at equilibrium estrone concentration of 5.9 ng/L. The performance of the hybrid PS nanoparticle-UF system was studied in terms of adsorption and membrane permeability under varying solution pH, particle size and particle concentration. The results indicated that neutral pH range is optimal for operation of the system and estrone removal with nanoparticles above 465 nm is negligible. The highest estrone removal (40%) was achieved by the hybrid system using a 100 kDa UF membrane and 84 mg/L PS (52 nm) nanoparticle concentration. The capacity of the system to remove estrone was found to be lower than most nanofiltration/reverse osmosis (NF/RO) systems but with a final permeability of 75 L/m2hbar, at least five times higher than most of the NF/RO systems.

KEYWORDS

Sorption; membrane filtration; polystyrene nanoparticles; ultrafiltration; estrone

1 Introduction

Hormones, both naturally secreted by human and animal bodies and synthetic, are known to be one of the most dangerous trace contaminant groups as they have high potential to disrupt the endocrine activities of living organisms [1]. The excreted or disposed hormones end up either in wastewater treatment plants (WWTPs) or directly in surface waters [2]. Current WWTPs are not able to remove hormones from water adequately [3] resulting in detected concentrations up to 275 ng/L in WWTP effluents [3-10], 195 ng/L in surface waters [11-13] and 120 ng/L in ground waters [14].

Even at such low concentrations, hormones can interfere with the endocrine regulatory systems of many living organisms causing disorders such as feminization of male fish [15-18] and increased risk of cancer in humans [19, 20] Synthetic and natural estrogens are suggested to be regulated as they are known as the most potent estrogenic compounds, however not regulation on the discharge is enforced as yet [21]. A recent rise in public awareness resulted in more studies conducted to explore efficient treatment processes for removing endocrine disrupting compounds from water [22].

While evaluating effective technologies, low energy requirement should be kept as one of the criteria considering that energy resources are becoming scarcer every day. The technologies showing promising results for the removal of hormones are advanced oxidation/ozonation processes (AOPs) [22, 23] and nanofiltration/reverse osmosis (NF/RO) [24-26]. Nevertheless, NF/RO systems have high energy requirement ~1 kWh/m^3 [27] whereas AOPs are susceptible to formation of toxic by-products [28-31] which contribute to residual estrogenic activity in the treated water [32, 33]. The removal of hormone with NF/RO systems varies between 8% and 99% [24, 26, 34, 35] depending on the membrane and hormone characteristics as well as the operational parameters, while the permeate hormone

concentration varies between <1 ng/L and 883 ng/L [24, 26, 34, 35] depending on the removal efficiency and the feed hormone concentration.

Recently, hybrid activated carbon-low pressure membrane systems were investigated as an alternative technology [36-38]. The energy requirement of looser membrane systems such as ultrafiltration is 0.1-0.2 kWh/m^3 [39, 40], an order of magnitude less than the ~1 kWh/m^3 required for NF/RO systems [27]. Although activated carbon seems to be an efficient sorbent for hormones [41-44] the thermal regeneration required can be highly energy consuming [45]. Due to the relatively easy regeneration characteristics and the availability of functionalisation methods, polymeric sorbents are often indicated as potentially better candidates than activated carbon [46]. High sorption of hormones on non-polymeric nanomaterials has been reported recently [47-49] showing high potential for water treatment applications [50] and has been attributed to their large surface area. Nano size polymer sorbents can be a promising compromise for hormone removal combining high surface area with functionalisation and easy regeneration. Effective sorption of steroid hormones on resins made of cross-linked polystyrene divinylbenzene (PS-DVB) has been reported [51].

In this study, a hybrid polystyrene (PS) nanoparticle-UF system was studied for the removal of hormones from water. PS nanoparticles were employed, firstly because they provide a large surface area due to their nano-size and, secondly, because they can easily be manufactured in different sizes and functionalized. Moreover, non-porous and chemically resistant PS particles would enable easy regeneration of the materials. Treatment with organic solvents, bases or acids, steam, supercritical fluids or microwave radiation are among the methods used for the regeneration of the spent polymeric sorbents [46]. Hormone sorption capacity of the plain PS nanoparticles at environmental hormone concentrations has not been studied before and such a study can give an indication on the mechanisms underlying sorption on nanoparticles and where to act to improve the system performance.

This work aims to investigate the fundamental design parameters of the hybrid PS nanoparticle-UF system and evaluate the performance in comparison to NF/RO technologies in terms of hormone removal and membrane permeability. One of the major limitations in UF is fouling which results in deterioration in membrane performance. The system performance was studied with changing: particle size, particle concentration, solution pH and molecular weight cut off (MWCO) of the UF membrane. All of these parameters can potentially influence both hormone adsorption onto the particles and membrane permeability.

2 Materials and Methodology

2.1 Solution Chemistry and Hormones

Analytical grade chemicals and ultra-pure water (conductivity: 18.2 mS/cm) obtained by PuraLab Ultra (Elga LabWater, UK) were used to prepare the solutions. The pH of the solutions was adjusted with 1M HCl and 1M NaOH (Fisher, UK). Nanoparticle characterisation and experiments were conducted in background electrolyte solution of 1 mM $NaHCO_3$ and 20 mM NaCl (Fisher, UK).

Estrone (E1) (MW: 270.4 g/L [52]) solutions were prepared using tritium labelled [2, 4, 6, 7-3H] estrone (2.449 TBq/mmol with a radioactive activity of 37 MBq/mL (Perkin Elmer, UK). Non-labelled estrone (≥ 98% purity) (Sigma Aldrich, UK) was used together with the tritium labelled estrone where needed for preparing the solutions with concentrations ≥500 ng/L. The radioactivity of estrone was measured in disintegration per minute (dpm) with a Beckman LS 6500 scintillation counter (Fullerton, USA) after mixing 0.5 mL of sample with 3.5 mL of Ultima Gold LLT (Perkin Elmer, UK) in 20 mL scintillation vials (Perkin Elmer, UK). Each sample was measured three times, each for a duration of 10 minutes, and the average value was reported. The instrument was calibrated each time a new hormone stock solution was prepared.

2.2 Nanoparticle Characterization

Plain (52, 81, 465 and 3000 nm) and fluorescent (43 nm) PS nanoparticles (Polysciences Inc., Germany) were used. Prior to experiments and instrumental analysis, the nanoparticle solutions were sonicated for 5-10 seconds with 150 W ultrasonic cleaner (Sonic Wave, UK) to break any possible aggregates.

The effective diameter and zeta potential measurement of the nanoparticles were determined by 90Plus/BI-MAS Particle Size and Zeta Plus (Brookhaven Instruments, New York, USA), respectively, by taking the mean of 10 measurements. Prior to the measurements, the samples were allowed to equilibrate at the temperature of the sample holder in the instrument for at least five minutes. Concentrations of ~0.60 % v/v for 43 nm, 52 and 81 nm and 0.15 % v/v for 465 and 3000 nm size were used for the zeta potential measurements of PS nanoparticles.

The size and the surface charge of the particles are presented in Table 1. Particle sizes provided by the manufacturer were used in the analysis as the values were confirmed by the measurement conducted with particle size analyser and scanning electron microscopy (SEM). The microscope images of 52, 81 and 465 nm particles confirm that the particles are spherical, uniform and have a narrow size distribution as can be seen in the Supporting Information Figure S-1. Zeta potential values show that the absolute surface charge of the particles with larger size (465 and 3000 nm) is higher compared to 43, 52 and 81 nm particles. Higher zeta potential for larger PS particles was also reported by Elimelech [53] and was attributed to the higher surface charge density [54].

Table 1 Characterization of the PS nanoparticles

Diameter[a] (nm)	43±5.9 (fluorescent)	52±7.9	81±10	465±11	3000±65
Diameter[b] (nm)	49.1±2.5	49.0±2.5	71.8±3.7	469.8±23.9	−
Diameter[c] (nm)	−	49.4±9.8	73.3±17.7	476.1±17.9	−
Zeta Potential[b] (mV)	-62.7±8.0	-52.2±6.7	-64.1±8.2	-106.7±13.7	-92.9±11.9

[a] according to the manufacturer, [b] measured in 20 mM NaCl and 1 mM $NaHCO_3$ with size analyser, [c] size obtained from SEM images

Constant zeta potential values for 52 nm particles, presented in Supporting Information Figure S-2, imply that solution pH between 3 and 12 does not influence the surface charge of the particles agreeing well with other studies [53, 54].

2.3 Membranes

PL series UF membranes (Millipore, US) made of a regenerated cellulose active layer on a polypropylene support were used in the experiments. Regenerated cellulose membrane was selected due to its known minimal hormone sorption [55]. Prior to use, the membrane coupons were soaked in 0.1 M NaOH (Fisher, UK) solution for 30 minutes to remove the glycerine preservative present on the surface. Afterwards they were rinsed with plenty of tap water followed by 2.5 L of ultra-pure water. Prior to the filtration experiments, the membranes were compacted for 30 minutes and the pure water flux of the membrane was determined over the following hour.

The membrane characteristics and the operational conditions for the permeation tests are presented in Table 2.

Table 2 UF membrane characteristics and operational conditions

MWCO	Pore Diameter[a]	Pore Diameter[b]	Operating Pressure	Average Pure Water Flux	Pure Water Permeability	Clean Membrane Resistance[c]
kDa	Nm	Nm	Bar	$L/m^2.h$	$L/m^2.h.bar$	1/m
1	1.59	2.64	5	22±4	4	8.27E+13
3	2.84	4.37	5	39±5	8	4.69E+13
5	3.72	5.53	5	56±9	11	3.24E+13
10	5.37	7.61	5	109±9	22	1.68E+13
30	9.62	12.6	1	326±19	326	1.07E+12
100	18.2	21.9	0.5	433±55	865	4.30E+11

[a] estimated after Worch [56, 57], [b] estimated after Crittenden et al. [58] [c] calculated with Equation 4 using average operation temperature (21 °C),

The MWCO of the membranes were chosen in order to have no size exclusion for E1 with an equivalent molecular width of 0.76 nm [52] and no penetration of the particles in the membranes as the smallest particle size (43±5.9 nm) is at least two times larger than the largest average pore size (Table 2).

2.4 Batch Adsorption Protocol

PS nanoparticles were added to 100 mL of pH adjusted estrone solutions and the solutions were mixed for an hour at 200 rpm at 20 ºC in a Certomat BS-1 orbital shaker (Sartorius, Germany). The adsorption equilibrium for PS particles was reached within 50 minutes as determined in the preliminary studies (see Supporting Information Figure S-3). The solution was then subjected to ultra-centrifugation for four hours at 686700 m/s^2 (70,000xG) and 20 ºC in 16 mL polycarbonate centrifuge bottles (Beckman Coulter, UK).

Concentration of the fluorescence-labelled nanoparticles in solution was determined by measuring the peak ultraviolet absorbance at 444 nm for the yellow green dye using a Cary 100 Scan ultra-violet visible spectrophotometer (Palo Alto, USA). By varying centrifugation time and measuring absorbance in the supernatant solution, it was determined that four hours ensured that >95% nanoparticles settled. The absorbance was measured at different fluorescent PS concentrations after centrifugation for four hours and a correlation curve was obtained between the PS particle concentration (mg/L) and the YG dye absorbance.

E1 concentrations in initial and supernatant samples were analysed in order to determine the amount of hormone adsorbed.

2.5 Stirred Cells and Filtration Protocol

166 The dead end filtration experiments were conducted using stainless steel stirred cells with a
167 cell volume of 990 mL and a membrane holder with a membrane surface area of 0.0033 m^2
168 exposed to the solution. The cells contained a magnetic stirrer assembly (Millipore, UK) and
169 were operated at 300 rpm placed on a magnetic stirrer (Fisher Scientific, UK). The permeate
170 from each cell was collected in a beaker placed on an electronic balance (Fisher Scientific,
171 Loughborough, UK) and the mass of the permeate was monitored continuously. The cells
172 contained a pressure transducer (PX209-300G5V) and a thermocouple (TJ2-CPSS-M6OU-
173 200-SB) which were connected to a data acquisition system (OMB-DAQ-56), all purchased
174 from Omega Engineering (UK). The data from the acquisition system and the balance were
175 transferred to a computer and processed using LabVIEW 8.0 software (National Instruments,
176 UK).

177 PS nanoparticles at varying concentrations were mixed into 100 mL ultra-pure water and the
178 solution was filtered completely until all the particles were deposited on the membrane
179 surface. Following the deposition, the ultra-pure water flux of the membrane with
180 nanoparticle deposit was recorded for an hour. For all the membrane filtration experiments,
181 450 mL of 100 ng/L E1 feed solution was filtered and 8 samples of 50 mL permeate were
182 collected until 50 mL of concentrate sample was left in the cell. E1 concentration in feed,
183 permeate and the concentrate samples were analysed. Membrane sorption (blank)
184 experiments were performed using the same protocol without nanoparticle deposition.

185 2.6 Nanoparticle Deposit Characterization

186 The membranes with nanoparticle deposit layers were preserved in a petri dish on a wet
187 cotton tissue to prevent the membranes and the deposit from drying out. Imaging of the
188 particle deposit was conducted using Supra 40V scanning electron microscopy (SEM) (Carl
189 Zeiss, UK) with a beam voltage of 1 kV and a freeze drying unit (Quorum Technologies,
190 UK). Three square pieces of membrane, each with the size of about 5 to 5 mm, were cut with

a spatula from different locations of the membrane coupon with deposited nanoparticles. All three pieces were placed between two silicon plates at the same time and the silicon plates were clamped perpendicular to a sample holder in order to image the cross sections. The sample holder was connected to a transfer rod and was immersed in liquid nitrogen for about half a minute until the temperature on the holder was between -80 and -100 °C. The holder was then closed and transferred to the freeze drying unit without any contact to the air. In the freeze drying unit, the samples were allowed to dry at low temperature under vacuum (~2.67 Pa) for about 2.5 hours. When the samples were warmed up to 3-5 °C, the samples were transferred into the imaging chamber and imaged without coating. The thicknesses of the nanoparticle deposit layers were determined from the SEM images using the program Image J_1.40.

2.7 Data Analysis

For the batch experiments, E1 mass adsorbed, m_{ads} (ng) on PS nanoparticles was calculated with a simple mass balance (Equation 1) where V_i is the initial volume (L) of the solution, C_i and C_s are the initial and supernatant E1 concentrations (ng/L) respectively, and m_{tube} is the mass adsorbed onto the centrifuge tube.

$$m_{ads} = (C_i - C_S)V_i - m_{tube} \quad (1)$$

m_{tube} for each experiment was determined by conducting batch experiments without nanoparticles in the centrifuge tube.

For the filtration experiments, E1 mass adsorbed, M_{ads} (ng) on PS nanoparticles was calculated with Equation 2 where V_f, V_P and V_c are the volume (L) of feed, permeate and concentrate, respectively, C_f, C_{Pi} and C_c are the E1 concentration (ng/L) of feed, sample permeate and concentrate, respectively, m_{mem} is the E1 mass adsorbed on the membrane, and $_i$ is the identity number of permeate samples.

$$M_{ads} = V_f.C_f - \sum_i^8 V_{p_i}.C_{p_i} - V_c.C_c - m_{mem} \quad (2)$$

m_{mem} was determined with blank experiments, where no nanoparticles were added to the system.

The nanoparticle surface area available (SA_{PS}) was calculated using Equation 3 where c_f is the particle feed concentration (g/L) in the cell, ρ_p is the PS particle density provided by the manufacturer (1.05 g/cm^3) and d_p is the particles diameter (cm). c_f and V_f were replaced by x_f and V_i, respectively for the surface area calculations of batch adsorption experiments, where x_f is the initial particle concentration in the centrifuge tube.

$$SA_{PS} = \frac{6c_f V_f}{\rho_p d_p} \quad (3)$$

Deposit resistance of the nanoparticles (R_d) (1/m) was determined with ultra-pure water filtration and calculated using Equation 4, where J is the water flux (L/m^2.h), L_v is the water permeability (L/m^2.h.bar), ΔP is the hydrostatic pressure difference (bar), μ is the dynamic viscosity (converted into bar.h) of water at the experimental temperature (21±2 °C), and R_m is the membrane resistance (1/m). R_m was calculated by using the flux data obtained from the experiments without particle deposition and Equation 4 [59]. The experimental flux for the experiments are reported in the Supporting Information (Table S-1).

$$L_v = \frac{J}{\Delta P} = \frac{1}{\mu(R_m + R_d)} 10^3 \quad (4)$$

According to deposit (cake) filtration theory, R_d can be calculated with Equation 5 [59-61] where δ is the deposit thickness (m) and δ_d is the maximum deposit thickness (m). In this study, an average porosity (ε) was calculated by using R_d determined experimentally, replacing d_p with the average nanoparticle diameter provided by the manufacturer and δ with average deposit thickness determined with SEM images.

$$R_d = \int_0^{\delta_d} \frac{180(1-\varepsilon)^2}{{d_p}^2 \varepsilon^3} d\delta \quad (5)$$

The deposit thickness (δ) determined using SEM images was compared to the deposit thickness value calculated with Equation 6, where M_d is the mass of particles in the deposit (g), ρ_p is the density of the nanoparticle (g/m^3), A_m is the membrane surface area (m^2) and ε is assumed as 0.4 (randomly packed deposit porosity) based on Carman-Kozeny calculations [59].

$$\delta = \frac{M_d}{\rho_p A_m (1-\varepsilon)} \quad (6)$$

M_d was calculated using Equation 7, where c_f, c_p, c_c are the concentrations of the nanoparticles in the feed, permeate and the concentrate respectively (g/L) and V_d is the volume of the particle deposit on the membrane surface. For the filtration experiments, c_c was assumed to be negligible ($c_c \approx 0$) since all the particles were deposited on the membrane before the solution filtration. Negligible c_c was confirmed by measuring the nanoparticle concentration in the concentrate using a portable turbidity meter TN-100 (Eutech Instruments, USA).

$$M_d = c_f V_f - c_p V_p - c_c (V_c - V_d) \quad (7)$$

In each data series for sorption and permeability, a single experimental data point was repeated at least three times and the variability was estimated by taking the largest difference among individual experimental data and the mean value.

3 Results

3.1 E1 Adsorption Capacity of PS Nanoparticles

Prior to studying the hormone adsorption in the proposed hybrid PS nanoparticle-UF system, E1 sorption on PS nanoparticles was studied with batch experiments in order to understand

the limitations on the adsorption. E1 adsorption isotherms for particles at pH 7, 9 and 12 are shown in Figure 1.

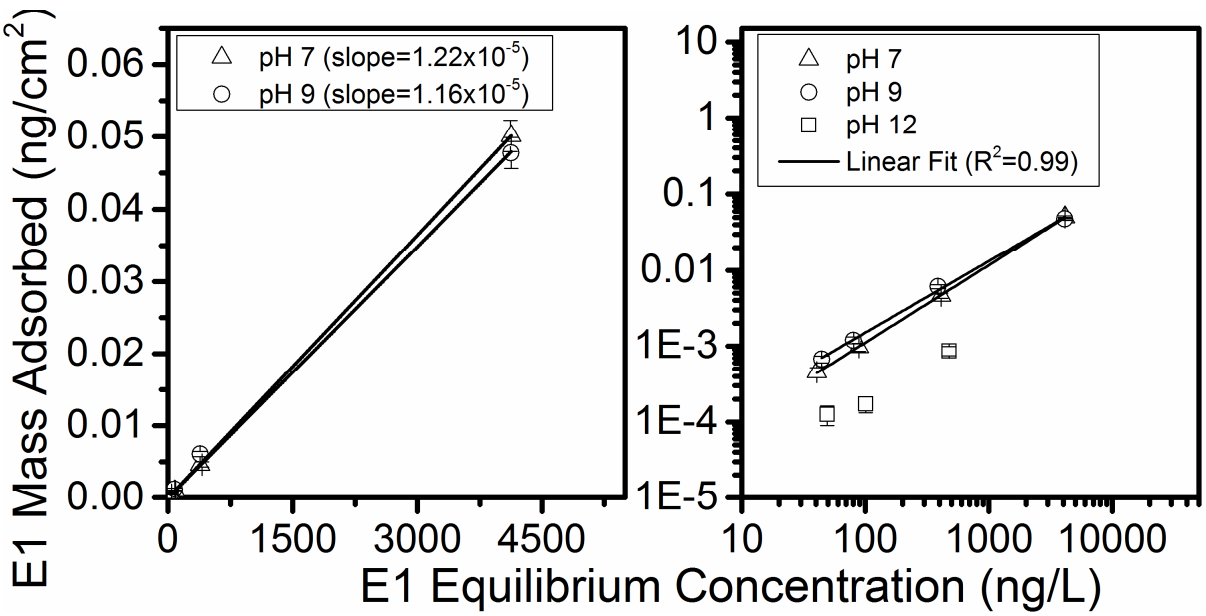

Figure 1 E1 adsorption isotherms of PS nanoparticles at pH 7, 9 and 12 on a logarithmic scale (right) and a linear scale (left). All batch experiments were performed with 16 mg/L PS (52nm) particle concentration, E1 solution with 1 mM $NaHCO_3$ and 20 mM NaCl background electrolyte

The adsorption capacity increased almost linearly with the equilibrium E1 concentration at solution pH 7 and 9. This linearity indicated that the active sites of the particles did not reach saturation within the E1 equilibrium concentration range of 50-5000 ng/L, hence the surface area was not a limiting factor for the studied E1 concentration range at 16 mg/L particle concentration. The linear isotherm is given in Equation 8 where Q is the E1 mass adsorbed on nanoparticles per particle surface area (ng/cm^2), C_e is the equilibrium E1 concentration and k is the adsorption constant (1.22x10^{-5} L/cm^2) obtained from the linear fit to the experimental data obtained at pH 7 (Figure 1) on a non-logarithmic scale.

$$Q = kC_e \quad (8)$$

At equilibrium concentration of 5.9 ng/L, the E1 adsorption capacity of 52 nm PS particles is 79.6 ng/g (7.20×10^{-5} ng/cm^2) which is higher than the estradiol sorption capacity of granular activated carbon reported in the literature as 47 ng/g (5.22×10^{-6} ng/cm^2) [41] indicating that PS nanoparticles are more efficient than activated carbon. The adsorption capacity is comparable at pH 7 and 9 (Figure 1) while a decline was observed as the solution pH was increased to 12. When the solution pH increases above the pK_a of E1 (10.23), neutral E1 dissociates and becomes negatively charged explaining the hindered adsorption at pH 12 due to the repulsion between the negatively charged E1 and PS particles.

Hydrophobic interactions are considered to play a big role in the E1 adsorption due to the hydrophobicity of the PS particles. On the other hand, at an equilibrium hormone concentration of 100 ng/L various resins made of PS-DVB have up to two orders of magnitude higher sorption capacity for estradiol (150 µg/g) [51] than the capacity of plain PS for E1 (1.35 µg/g). PS-DVB, a polystyrene crosslinked with divinylbenzene, is a hydrophobic polymer. The hydrophobicity of the PS-DVB varies depending on the degree of crosslinking [62], and the hydrophobicity of the internal and external surface area can be different [63]. It is likely that enhanced hydrophobicity and porosity due to the crosslinking of the PS particles can result in more hydrophobic interaction with the hormone molecules. Moreover, the π-π interactions can also contribute to the adsorption on crosslinked PS [64].

3.2 The Influence of PS Nanoparticle Size on E1 Adsorption and UF Permeability

E1 adsorption and UF permeability as a function of PS particle size are displayed in Figure 2. A trade-off between the adsorption and permeability is observed. Figure 2A shows that as expected, E1 mass adsorbed decreased with the increase in particle size forming the deposit due to the lower surface area available. At the same particle concentration, the smaller particle sizes (below 465 nm) provided larger amounts of active sites for the E1. For the particles larger than 465 nm, the surface area available became so small that E1 adsorption

was negligible. In order to check whether or not the linear sorption isotherm obtained during the batch adsorption experiments apply also to the filtration experiment data, E1 mass adsorbed was estimated based on the linear isotherm (Equation 8) using the equilibrium E1 concentrations obtained in the filtration experiments. The estimated results, given in Figure 2A, agree with most of the data except for the smallest (52 nm) PS particles at 50 mg/L. Under this particular condition, the experimental results lie outside the expected trend with a small difference compared to that observed for 81 nm particles. The reason for this is not completely understood. The available surface area for 52 nm PS particles at 50 mg/L was the largest in the series and the estimated E1 mass adsorbed based on the linear sorption isotherm was larger than the E1 mass adsorbed obtained in the filtration experiment.

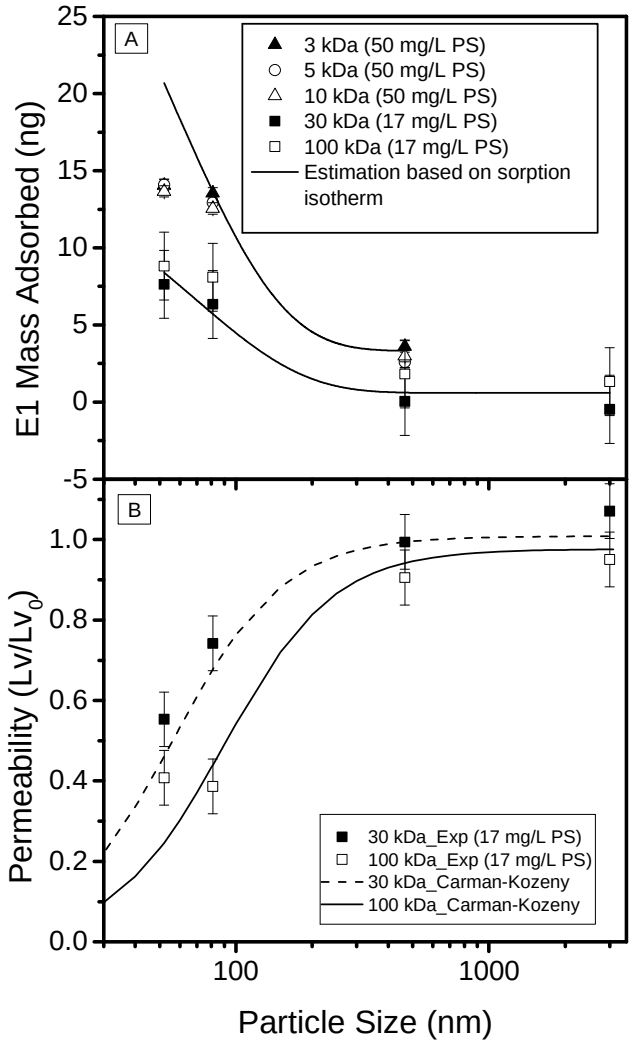

301

302 **Figure 2** The influence of particle size on A) E1 adsorbed and B) permeability: filtration
303 experiments with 52, 81, 465 and 3000 nm particles, 17 and 50 mg/L PS particle
304 concentration, 100 ng/L E1 solution with 1 mM $NaHCO_3$ and 20 mM NaCl background
305 electrolyte, pH 7. Carman-Kozeny model with the assumption, deposit porosity is 0.4
306 (independent of particle size). Estimation based on the sorption isotherm obtained with the
307 batch experiments and the experimental equilibrium E1 concentration

308 The permeability declined as the size of the particles forming the deposit decreased for both
309 30 and 100 kDa membranes as shown in Figure 2B. Permeability data for 3, 5 and 10 kDa are
310 not presented as no change was observed with these smaller MWCO membranes. The decline
311 in permeability of 30 and 100 kDa membranes can be explained by the increased deposit

resistance. The calculated deposit resistance for different particle size is presented in Figure 3. The results show that the deposits formed on 30 and 100 kDa membranes exert similar resistances, as the differences between them are within experimental error. The higher permeability decline for the 100 kDa membrane compared to the 30 kDa one (Figure 2B) can be attributed to the intrinsic membrane resistance that is an order of magnitude smaller for the 100 kDa membrane (Table 2). As can be seen in Equation 4, the overall resistance is the sum of R_m and R_d and inversely proportional to the permeability; hence the change in permeability will be larger for a membrane with a lower R_m if the resistance due to the deposit is the same.

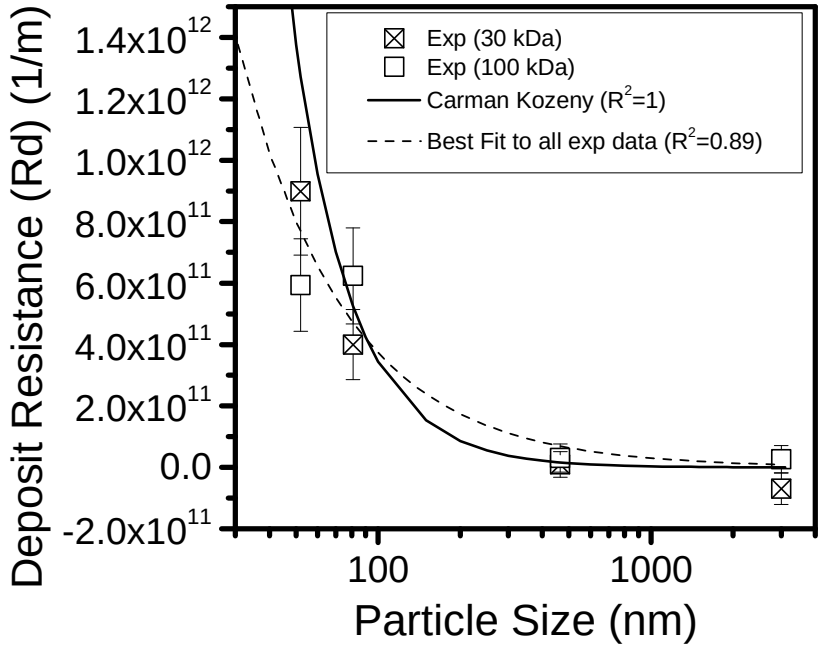

Figure 3 Deposit resistance with changing PS particle size: filtration experiments, 52, 81, 465 and 3000 nm particles, 17 mg/L PS concentration, 100 ng/L E1 solution with 1 mM $NaHCO_3$ and 20 mM NaCl background electrolye, pH 7. Carman-Kozeny calculations assumptions, porosity is 0.4 (randomly packed deposit), 100% particle mass retention (7.1 mg), homogenous and constant deposit thickness

Using the best fit line to the resistance data in Figure 3, an empirical relationship is obtained between the particle size forming the deposit and the resistance applied by the deposit. The

relationship is found to be a simplified version of the Carman-Kozeny equation (Equation 5) and is formulated into Equation 9, where R_d is deposit resistance (1/m), a and b are coefficients and d_p is the particle diameter (nm). Coefficients a and b are obtained from the best fit of the R_d data against the particle size and they are 2.0×10^{14} and 1.36 respectively.

$$R_d = \frac{a}{d_p^{\,b}} \tag{9}$$

Coefficient a can be expressed as in Equation 10, where it is dependent on the deposit porosity (void fraction) and the average deposit thickness (m).

$$a = \frac{180(1-\varepsilon)^2}{\varepsilon^3}\delta \tag{10}$$

In the Carman-Kozeny equation, the deposit resistance is inversely proportional to the square of the particle size (d_p^2). Experimentally, however, the coefficient b which represents the power of particle size was found to be 1.36. The fact that this is substantially less than 2.0 indicates that the experimental data do not agree with the Carman-Kozeny in this respect. Deposit resistance estimated by the Carman-Kozeny equation tends to underestimate the contribution of larger particles and overestimate the effect of smaller particles which agrees with the literature [65]. Lee and Clark [65] suggest that one possible reason for the overestimation of the specific deposit resistance for smaller particles is the increased porosity of the deposit thickness due to the aggregation of the smaller particles and formation of larger primary particles. However, in this study, the measured zeta potential values of 52 nm particles (Table 1) indicate that the particles are stable and do not tend to aggregate. The second reason stated by Lee and Clark [65] is the increase in the volume occupied by the double-layer of the smaller particles, hence porosity, due to their larger surface area as the particle size decreases. This second reason is more likely to explain the over and underestimation of the deposit resistance in this study.

3.3 The Influence of PS Nanoparticle Concentration on E1 Adsorption and UF Permeability

Figure 4A shows that E1 mass adsorbed is not dependent on the MWCO of the UF membrane used in the system.

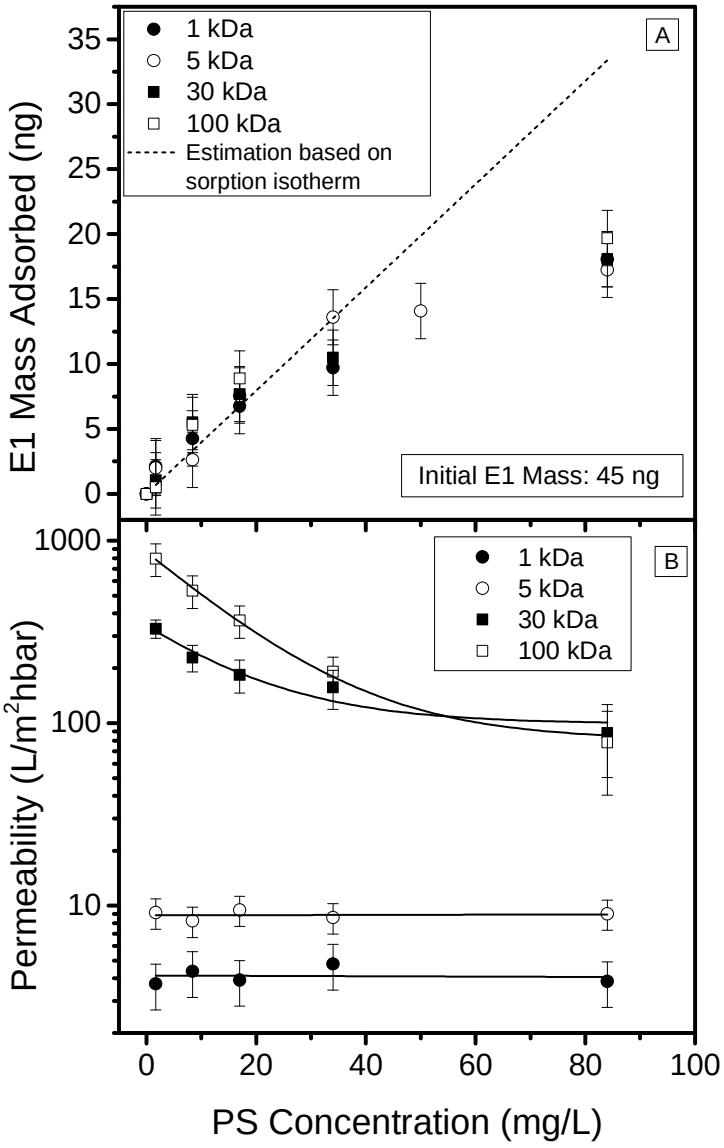

Figure 4 The effect of PS concentration on; A) E1 mass adsorbed and B) permeability of different MWCO UF membranes: filtration experiments, 1.7, 8.4, 17, 34 and 84 mg/L PS (52 nm) concentration, 100 ng/L E1 concentration with 1 mM $NaHCO_3$ and 20 mM NaCl background electrolyte, pH 7. Estimation based on the sorption isotherm obtained with the batch experiments and the experimental equilibrium E1 concentration

The E1 mass adsorbed achieved in the membrane filtration system at varying particle concentration was compared with the E1 mass adsorbed estimated with the linear isotherm (Equation 8) based on the equilibrium E1 concentrations of the filtration experiments. The filtration results agree well with the estimation based on the linear isotherm only up to particle concentration of 17 mg/L, above which the isotherm seems to overestimate the E1 mass adsorbed in the filtration system. This overestimation is likely due to the differences in the dynamics of the batch and the filtration systems.

In order to understand the kinetics of the E1 adsorption in the system better, the change in the permeate E1 concentration was studied for each MWCO membrane with different initial particle concentrations. When the E1 permeate concentration for each MWCO is plotted against time (Figure 5), it is observed that the sorption equilibrium with different membranes is reached at different times. However, it has to be noted that, in a dead-end filtration system, PS cell concentration increases with time and the rate of increase depends on the MWCO of the membrane. Each MWCO membrane has a different flow rate, thus the system reaches the same PS cell concentration at different times even if the initial PS concentration is the same.

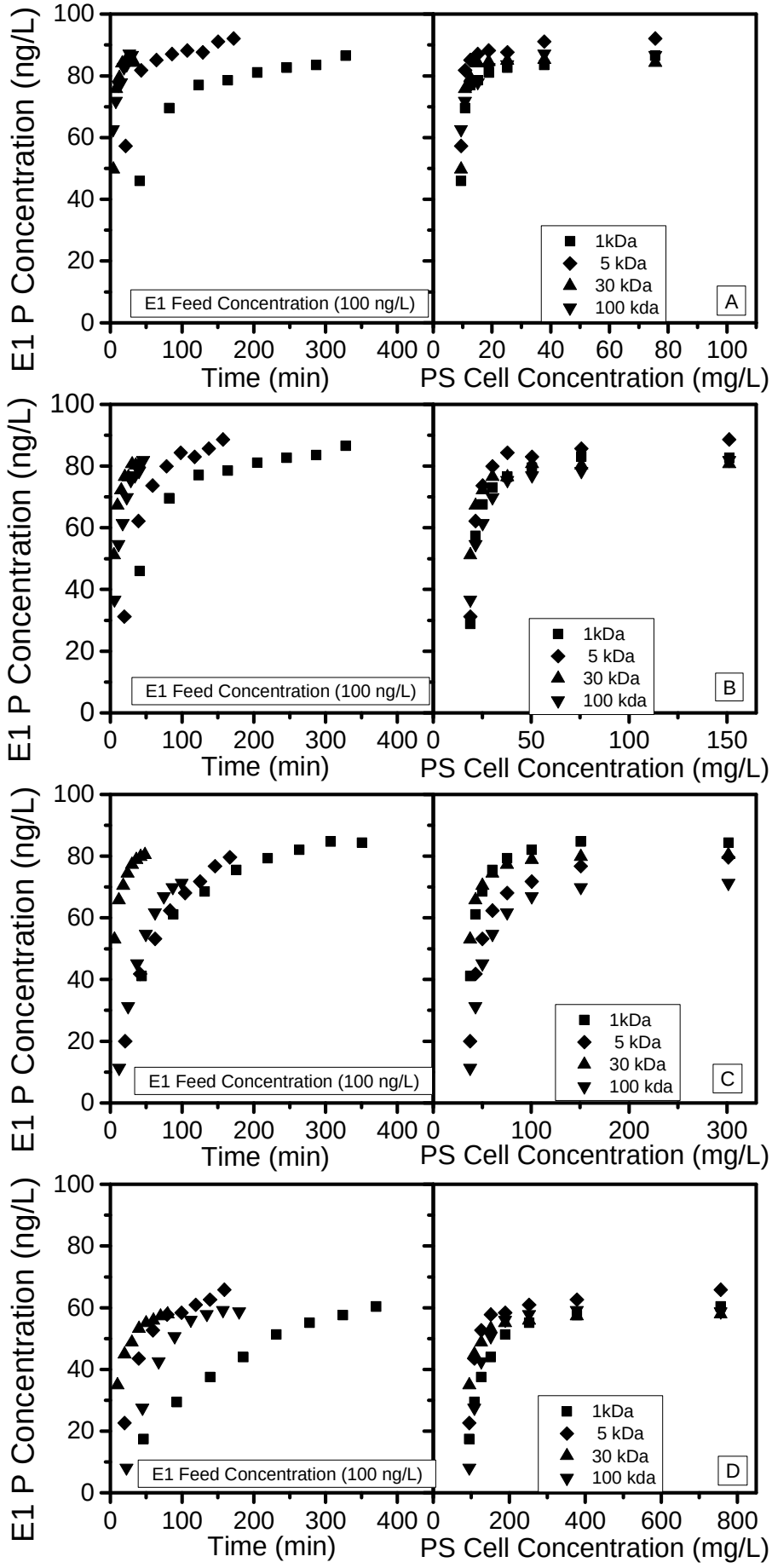
E1 P Concentration (ng/L)
Time (min)
PS Cell Concentration (mg/L)
E1 Feed Concentration (100 ng/L)
1kDa
5 kDa
30 kDa
100 kda
A
B
C
D

376

Figure 5 Permeate (P) E1 concentration change as a function of time (left) and with respect to PS concentration in the cell (right) with different initial PS (52 nm) concentration: 8.4 mg/L (A), 16.8 mg/L (B), 33.5 mg/L (C) and 84 mg/L (D): filtration experiments, 100 ng/L E1 concentration with 1 mM $NaHCO_3$ and 20 mM NaCl background electrolyte, pH 7

PS cell concentration is calculated for each sampling time and the E1 permeate concentration is re-plotted against this parameter. It is then observed for all membranes studied that adsorption equilibrium is reached at the same PS cell concentration. Furthermore, the specific PS cell concentration at which adsorption equilibrium is reached increases with the initial PS concentration. Unlike in the batch system, variation in PS nanoparticle and E1 concentration in the cell due to the nature of filtration, alters the adsorption and desorption equilibrium. Nghiem [66] stated that the increase in the recovery of the water in dead end filtration systems resulted in an increase in the release of the hormones from the NF membrane. Hormone concentrations in the permeate were thus increased due to the concentration build up at the membrane surface and ineffective back diffusion. In this study, the deposit layer formed by PS particles acts as another membrane layer on top of the UF and the high concentration of the E1 on the deposit layer due to the adsorption can cause a similar increased release effect to the permeate. As can be seen in Figure 5, after the initial decline, E1 permeate concentration starts to increase until it reaches the equilibrium. The increase in E1 permeate concentration can possibly be attributed to the release of the hormones from the particles, increased concentration at the membrane surface and diffusion to the permeate side as the E1 mass adsorbed increases in the PS layer.

Results, presented in Figure 4B, show that the permeability declines for 30 and 100 kDa membranes as the PS concentration increases due to the increase in the deposit resistance. A linear relationship between the feed mass of the particles and the deposit resistance for both 30 and 100 kDa membranes confirmed the cake filtration theory.

In order to fully understand the reason behind the increase in deposit resistance, the thickness of the deposit on 100 kDa membrane at three different initial PS concentrations was imaged with SEM; some of the images are presented in Supporting Information Figure S-4. The measured average thickness and the specific deposit resistance values are given in Figure 6. The linear increase of the thickness values and the constant specific deposit resistance values confirm that the increase in the deposit resistance is clearly due to the increased deposit thickness. Based on the measured thickness values, porosity was calculated as 0.53±0.08, 0.48±0.06 and 0.46±0.06 for each initial particle concentrations of 8.4, 17 and 34 mg/L, respectively. The calculated values show that the deposit porosity does not depend on the initial particle concentration at constant applied pressure indicating that the cake is not compressible. This is consistent with the hypothesis of Lee and Clark [65].

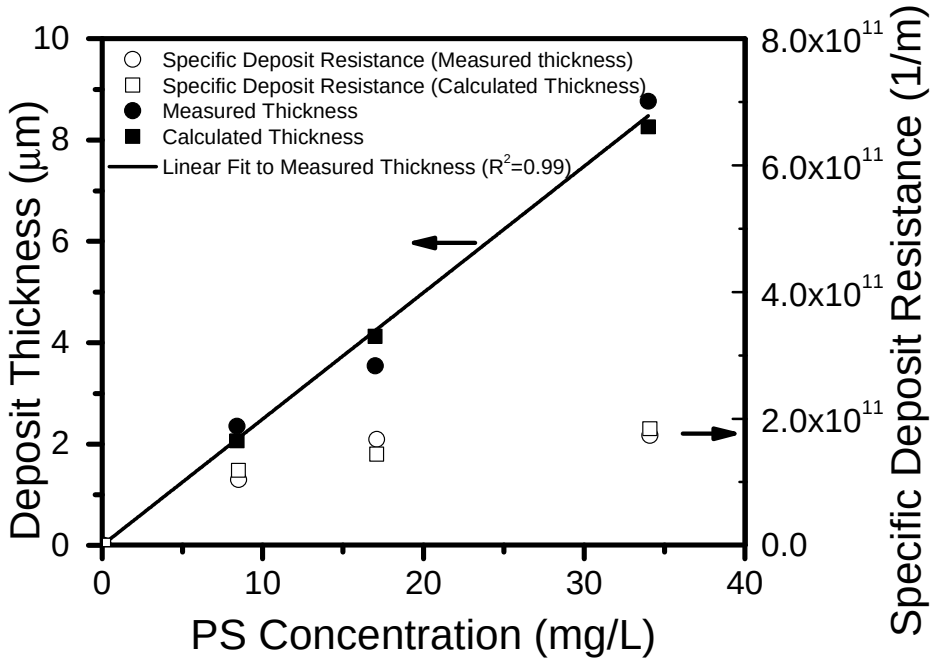

413

414 **Figure 6** The change in specific deposit resistance and deposit thickness with feed PS
415 concentration on 100 kDa membrane: filtration experiments, 8.4, 17 and 34 mg/L PS (52 nm)
416 concentration

417 3.4 The Influence of Solution pH on E1 Adsorption and UF Permeability

418 The influence of solution pH on E1 adsorption and membrane permeability is presented in
419 Figure 7A and 7B respectively. E1 adsorption is lower on PS nanoparticles at solution pH
420 above 10 due to electrostatic repulsion between the deprotonated E1 (pK_a:10.3 for E1) and
421 the negatively charged PS particles. The results agree well with the results of the batch
422 adsorption experiments conducted only with PS nanoparticles at varying pH (Figure 1).

423 As it can be seen in Figure 7B, the deposit resistance does not change with changing pH
424 indicating that there is no influence of pH on the deposit packing density.

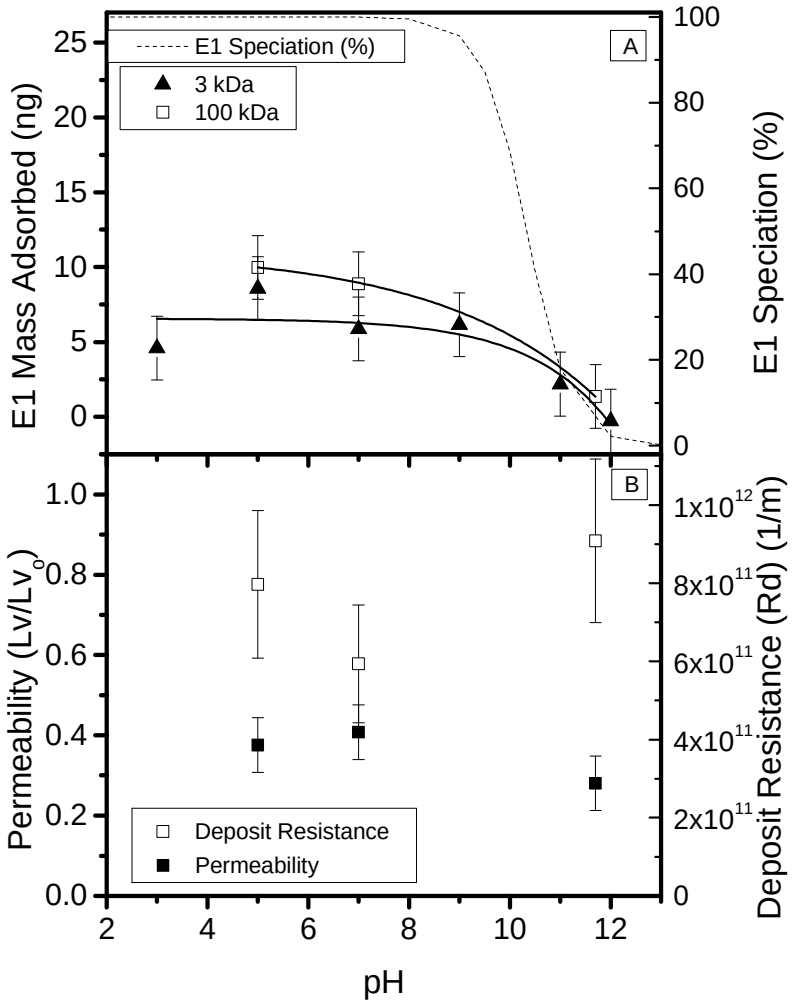

Figure 7 The influence of pH on: A) E1 mass adsorbed for 3 and 100 kDa B) Permeability and deposit resistance for 100 kDa. Filtration experiments: 17 mg/L PS (52 nm) concentration, 3 and 100 kDa, 100 ng/L E1 solution with 1 mM $NaHCO_3$ and 20 mM NaCl background electrolyte, pH 7

As the surface charge of the PS nanoparticles remains the same within the pH range, the interaction behaviour of the particles is not expected to change. The isoelectric point for the 100 kDa membrane is between pH 3 and 4. The surface charge of the membrane decreases from -12.5 to -20 mV as the pH increases from 5 to 10 respectively. The repulsion between the particles and the membrane might increase as the pH increases and fewer particles may accumulate in the deposit; however, this is not observed in this study. Permeability and deposit

436 resistance data for 3 kDa membranes are not presented as no change was observed with such a
437 small MWCO membrane.

438 4 Conclusions

439 The hybrid PS nanoparticle-UF system achieved a E1 removal capacity of 40% and a final
440 permeability of 75 L/m^{2}hbar when operated with 100 ng/L initial E1 concentration and 84
441 mg/L PS (52 nm) nanoparticle concentration. E1 removal of 40% is comparable to some but
442 lower than most of the NF/RO systems but the permeability is at least five times higher than
443 for most of the NF/RO systems. Although the estrone removal capacity of the hybrid system
444 with 100 kDa MWCO membrane was the same as the ones obtained with other MWCO
445 membranes, 100 kDa membrane provided the highest permeability with the deposited PS
446 nanoparticles, hence is recommended for further research.

447 Solution pH does not play a role on E1 sorption or UF permeability as long as it is below the
448 pK_a values of the hormones. The permeability of the 100 kDa membrane with 52 nm particles
449 deposit is not influenced by pH due to the stable particle surface characteristic. Considering
450 that some NF and RO systems can remove E1 up to 99 %, a feasible and competitive hybrid
451 technology can only be achieved by employing nanoparticles with higher sorption affinity.
452 Surface functionalized PS nanoparticles can provide the required high sorption affinity and are
453 recommended for further research. It is also recommended that the most feasible regeneration
454 method is selected and optimized in order to design the hybrid system effectively.

Acknowledgment

The PhD research of Ime Akanyeti was funded by EPSRC/RSC Analytical Studentship and Dalton Research Institute DRIAM Analytical Service has provided the financial support for nanoparticle deposit characterisation with FE-SEM. Prof. Andrea I. Schäfer, Karlsruhe Institute of Technology, is acknowledged for initiating the project and valuable scientific discussions. We thank Dr Chris Jeffree from the University of Edinburgh and Dr Vladimir Vishnyakov from Manchester University for developing the method for FE-SEM analysis of nanoparticle deposit on membrane surface, Dr. Greg Anderson from the University of Edinburgh for assisting to use the ultracentrifuge, Zuzanna Kamasa for helping with some of the experimental work, Dr. Ben Corry from the Australian National University for assistance in some of the method development of nanoparticle analysis, Dr. Helen Cope, University of Edinburgh, for proof reading, and Millipore Corporation for kindly supplying the membranes used for the experiments.

References

1. Wenzel, A., M. J., and T. Thomas, *Study on endocrine disrupters in drinking water. Final report: ENV.D.1/ETU/2000/0083*. 2003, Institute for Molecular Biology and Applied Ecology (IME) and Institute for Water Research and Water Technology (JOGU-ESWE) Germany.
2. Heberer, T., *Occurrence, fate, and removal of pharmaceutical residues in the aquatic environment: a review of recent research data.* Toxicology Letters, 2002. **131**(1–2): p. 5-17.
3. Sun, Y., et al., *Occurrence of estrogenic endocrine disrupting chemicals concern in sewage plant effluent.* Frontiers of Environmental Science & Engineering, 2014. **8**(1): p. 18-26.
4. Alda, M. and D. Barceló, *Review of analytical methods for the determination of estrogens and progestogens in waste waters.* Fresenius' Journal of Analytical Chemistry, 2001. **371**(4): p. 437-447.
5. Belfroid, A.C., et al., *Analysis and occurrence of estrogenic hormones and their glucuronides in surface water and waste water in The Netherlands.* Science of The Total Environment, 1999. **225**(1–2): p. 101-108.
6. Zhao, J.-L., et al., *Determination of phenolic endocrine disrupting chemicals and acidic pharmaceuticals in surface water of the Pearl Rivers in South China by gas chromatography–negative chemical ionization–mass spectrometry.* Science of The Total Environment, 2009. **407**(2): p. 962-974.
7. Desbrow, C., et al., *Identification of Estrogenic Chemicals in STW Effluent. 1. Chemical Fractionation and in Vitro Biological Screening.* Environmental Science & Technology, 1998. **32**(11): p. 1549-1558.
8. Ternes, T.A., et al., *Behavior and occurrence of estrogens in municipal sewage treatment plants — I. Investigations in Germany, Canada and Brazil.* Science of The Total Environment, 1999. **225**(1–2): p. 81-90.
9. Baronti, C., et al., *Monitoring Natural and Synthetic Estrogens at Activated Sludge Sewage Treatment Plants and in a Receiving River Water.* Environmental Science & Technology, 2000. **34**(24): p. 5059-5066.
10. Clara, M., et al., *The solids retention time—a suitable design parameter to evaluate the capacity of wastewater treatment plants to remove micropollutants.* Water Research, 2005. **39**(1): p. 97-106.
11. Liu, Z.-h., et al., *Occurrence, fate and removal of synthetic oral contraceptives (SOCs) in the natural environment: A review.* Science of The Total Environment, 2011. **409**(24): p. 5149-5161.
12. Al-Odaini, N.A., et al., *Multi-residue analytical method for human pharmaceuticals and synthetic hormones in river water and sewage effluents by solid-phase extraction and liquid chromatography–tandem mass spectrometry.* Journal of Chromatography A, 2010. **1217**(44): p. 6791-6806.
13. Liu, X., et al., *Analysis of hormone antagonists in clinical and municipal wastewater by isotopic dilution liquid chromatography tandem mass spectrometry.* Analytical and Bioanalytical Chemistry, 2010. **396**(8): p. 2977-2985.
14. Lapworth, D.J., et al., *Emerging organic contaminants in groundwater: A review of sources, fate and occurrence.* Environmental Pollution, 2012. **163**: p. 287-303.
15. Matozzo, V., et al., *Vitellogenin as a biomarker of exposure to estrogenic compounds in aquatic invertebrates: A review.* Environment International, 2008. **34**(4): p. 531-545.
16. Purdom, C.E., et al., *Estrogenic Effects of Effluents from Sewage Treatment Works.* Chemistry and Ecology, 1994. **8**(4): p. 275-285.
17. Leet, J.K., et al., *Environmental hormones and their impacts on sex differentiation in fathead minnows.* Aquatic Toxicology, 2015. **158**: p. 98-107.
18. Tetreault, G.R., et al., *Intersex and reproductive impairment of wild fish exposed to multiple municipal wastewater discharges.* Aquatic Toxicology, 2011. **104**(3–4): p. 278-290.

19. Diamanti-Kandarakis, E., et al., *Endocrine-Disrupting Chemicals: An Endocrine Society Scientific Statement.* Endocrine Reviews, 2009. **30**(4): p. 293-342.
20. Sharpe, R.M. and N.E. Skakkebaek, *Are oestrogens involved in falling sperm counts and disorders of the male reproductive tract?* Lancet, 1993. **341**(8857): p. 1392-1395.
21. WHO, *Fluorides and human health*, in *Monograph Series 59*. 1970, World Health Organization: Geneva.
22. Esplugas, S., et al., *Ozonation and advanced oxidation technologies to remove endocrine disrupting chemicals (EDCs) and pharmaceuticals and personal care products (PPCPs) in water effluents.* Journal of Hazardous Materials, 2007. **149**(3): p. 631-642.
23. Ikehata, K., N. Jodeiri Naghashkar, and M. Gamal El-Din, *Degradation of Aqueous Pharmaceuticals by Ozonation and Advanced Oxidation Processes: A Review.* Ozone: Science & Engineering, 2006. **28**(6): p. 353-414.
24. Comerton, A.M., et al., *The rejection of endocrine disrupting and pharmaceutically active compounds by NF and RO membranes as a function of compound and water matrix properties.* Journal of Membrane Science, 2008. **313**(1–2): p. 323-335.
25. Koyuncu, I., et al., *Removal of hormones and antibiotics by nanofiltration membranes.* Journal of Membrane Science, 2008. **309**(1–2): p. 94-101.
26. Nghiem, L.D., A.I. Schäfer, and T.D. Waite, *Adsorption of estrone on nanofiltration and reverse osmosis membranes in water and wastewater treatment.* Water Science & Technology, 2002. **46**(4-5): p. 265–272.
27. Larsen, T.A., et al., *How to avoid pharmaceuticals in the aquatic environment.* Journal of Biotechnology, 2004. **113**(1–3): p. 295-304.
28. Huber, M.M., T.A. Ternes, and U. von Gunten, *Removal of Estrogenic Activity and Formation of Oxidation Products during Ozonation of 17α-Ethinylestradiol.* Environmental Science & Technology, 2004. **38**(19): p. 5177-5186.
29. Alum, A., et al., *Oxidation of bisphenol A, 17β-estradiol, and 17α-ethynyl estradiol and byproduct estrogenicity.* Environmental Toxicology, 2004. **19**(3): p. 257-264.
30. Ohko, Y., et al., *17β-Estradiol Degradation by TiO2 Photocatalysis as a Means of Reducing Estrogenic Activity.* Environmental Science & Technology, 2002. **36**(19): p. 4175-4181.
31. Silva, C.P., M. Otero, and V. Esteves, *Processes for the elimination of estrogenic steroid hormones from water: A review.* Environmental Pollution, 2012. **165**: p. 38-58.
32. Bila, D., et al., *Estrogenic activity removal of 17β-estradiol by ozonation and identification of by-products.* Chemosphere, 2007. **69**(5): p. 736-746.
33. Guedes Maniero, M., D. Maia Bila, and M. Dezotti, *Degradation and estrogenic activity removal of 17β-estradiol and 17α-ethinylestradiol by ozonation and O3/H2O2.* Science of The Total Environment, 2008. **407**(1): p. 105-115.
34. Hu, J.Y., X. Jin, and S.L. Ong, *Rejection of estrone by nanofiltration: Influence of solution chemistry.* Journal of Membrane Science, 2007. **302**(1–2): p. 188-196.
35. Yoon, Y., et al., *Removal of endocrine disrupting compounds and pharmaceuticals by nanofiltration and ultrafiltration membranes.* Desalination, 2007. **202**(1-3): p. 16-23.
36. Chang, S., *Assessment of Trace Estrogenic Contaminants Removal by Coagulant Addition, Powdered Activated Carbon Adsorption and Powdered Activated Carbon/Microfiltration Processes.* J. Environ. Eng., 2004. **130**(7): p. 736.
37. Lee, S., et al., *Removal of 17β-estradiol by powdered activated carbon—Microfiltraion hybrid process: The effect of PAC deposition on membrane surface.* Journal of Membrane Science, 2009. **326**(1): p. 84-91.
38. Song, K.-Y., et al., *Coupling effect of 17β-estradiol and natural organic matter on the performance of a PAC adsorption/membrane filtration hybrid system.* Desalination, 2009. **237**(1–3): p. 392-399.

39. van Hoof, S.C.J.M., A. Hashim, and A.J. Kordes, *The effect of ultrafiltration as pretreatment to reverse osmosis in wastewater reuse and seawater desalination applications.* Desalination, 1999. **124**(1–3): p. 231-242.
40. Qin, J.-J., et al., *Dead-end ultrafiltration for pretreatment of RO in reclamation of municipal wastewater effluent.* Journal of Membrane Science, 2004. **243**(1–2): p. 107-113.
41. Fuerhacker, M., A. Dürauer, and A. Jungbauer, *Adsorption isotherms of 17β-estradiol on granular activated carbon (GAC).* Chemosphere, 2001. **44**(7): p. 1573-1579.
42. Fukuhara, T., et al., *Adsorbability of estrone and 17β-estradiol in water onto activated carbon.* Water Research, 2006. **40**(2): p. 241-248.
43. Li, F., et al., *Adsorption and biotransformation of 17β-estradiol in biological activated carbon adsorbers.* Adsorption, 2008. **14**(2-3): p. 389-398.
44. Valenzuela-Calahorro, C., et al., *Retention of Progesterone by an Activated Carbon: Study of the Adsorption Kinetics.* Adsorption, 2004. **10**(1): p. 19-28.
45. Snyder, S.A., et al., *Role of membranes and activated carbon in the removal of endocrine disruptors and pharmaceuticals.* Desalination, 2007. **202**(1-3): p. 156-181.
46. Wook Lee, J., H. Chul Park, and H. Moon, *Adsorption and desorption of cephalosporin C on nonionic polymeric sorbents.* Separation and Purification Technology, 1997. **12**(1): p. 1-11.
47. Pan, B., et al., *Adsorption and Hysteresis of Bisphenol A and 17α-Ethinyl Estradiol on Carbon Nanomaterials.* Environmental Science & Technology, 2008. **42**(15): p. 5480-5485.
48. Ji, L., et al., *Adsorption of Sulfonamide Antibiotics to Multiwalled Carbon Nanotubes.* Langmuir, 2009. **25**(19): p. 11608-11613.
49. Wang, F., et al., *Adsorption of sulfamethoxazole and 17β-estradiol by carbon nanotubes/CoFe2O4 composites.* Chemical Engineering Journal, 2015. **274**: p. 17-29.
50. Theron, J., J.A. Walker, and T.E. Cloete, *Nanotechnology and Water Treatment: Applications and Emerging Opportunities.* Critical Reviews in Microbiology, 2008. **34**(1): p. 43 - 69.
51. Hartmann, J., R. Beyer, and S. Harm, *Effective Removal of Estrogens from Drinking Water and Wastewater by Adsorption Technology.* Environmental Processes, 2014. **1**(1): p. 87-94.
52. Simon, A., et al., *Effects of caustic cleaning on pore size of nanofiltration membranes and their rejection of trace organic chemicals.* Journal of Membrane Science, 2013. **447**: p. 153-162.
53. Elimelech, M. and C.R. O'Melia, *Effect of particle size on collision efficiency in the deposition of Brownian particles with electrostatic energy barriers.* Langmuir, 1990. **6**(6): p. 1153-1163.
54. Tuin, G., J.H.J.E. Senders, and H.N. Stein, *Electrophoretic Properties of Monodisperse Polystyrene Particles.* Journal of Colloid and Interface Science, 1996. **179**(2): p. 522-531.
55. Han, J., et al., *Capturing hormones and bisphenol A from water via sustained hydrogen bond driven sorption in polyamide microfiltration membranes.* Water Research, 2012. **47**(1): p. 197-208.
56. Worch, E., *A new equation for the calculation of diffusion coefficients for dissolved substances (Eine neue Gleichung zur Berechnung von Diffusionskoeffizienten gelöster Stoffe).* Vom Wasser, 1993. **81**: p. 289-297.
57. Schäfer, A.I., *Natural organics removal using membranes. PhD*. 2000, The University of New South Wales: Sydney.
58. Crittenden, J.C., et al., *Water Treatment: Principles and Design*. 2005, New York: Wiley.
59. Carman, P.C., *Fundamental principles of industrial filtration.* Trans. Inst. Chem. Eng, 1938. **16**: p. 168-188.
60. Fane, A.G., *Ultrafiltration of suspensions.* Journal of Membrane Science, 1984. **20**(3): p. 249-259.
61. Zeman, L.J. and A.L. Zydney, *Microfiltration and Ultrafiltration, Principles and Applications*. 1996, New York: Marcel Dekker, INC. 618.

62. Molina, R., et al., *Wetting properties of polystyrene/divinylbenzene crosslinked porous polymers obtained using W/O highly concentrated emulsions as templates.* Surface and Interface Analysis, 2009. **41**(5): p. 371-377.
63. Penner, N., et al., *Investigation of the properties of hypercrosslinked polystyrene as a stationary phase for high-performance liquid chromatography.* Chromatographia, 1999. **50**(9): p. 611-620.
64. Davankov, V.A., et al., *Hypercrosslinked polystyrene as a novel type of high-performance liquid chromatography column packing material: Mechanisms of retention.* Journal of Chromatography A, 2003. **987**(1-2): p. 67-75.
65. Lee, Y. and M.M. Clark, *Modeling of flux decline during crossflow ultrafiltration of colloidal suspensions.* Journal of Membrane Science, 1998. **149**(2): p. 181-202.
66. Nghiem, L.D., *Removal of emerging trace organic contaminants by nanofiltration and reverse osmosis*. 2005, University of Wollongong: Wollongong.

Supporting Information

Hybrid Polystyrene Nanoparticle-Ultrafiltration System for Hormone Removal from Water

İme Akanyeti[a,b] *, Arno Kraft*[c] *and Maria-Chiara Ferrari*[a]*‡

[a] School of Engineering, University of Edinburgh, Robert Stevenson Road, Edinburgh EH9 3FB, UK

[b] Department of Environmental Engineering, Faculty of Engineering, Cyprus International University, Haspolat, Lefkoşa, North Cyprus, Mersin 10 Turkey

[c] Institute of Chemical Sciences, School of Engineering and Physical Sciences, Heriot-Watt University, Edinburgh, EH14 4AS, UK

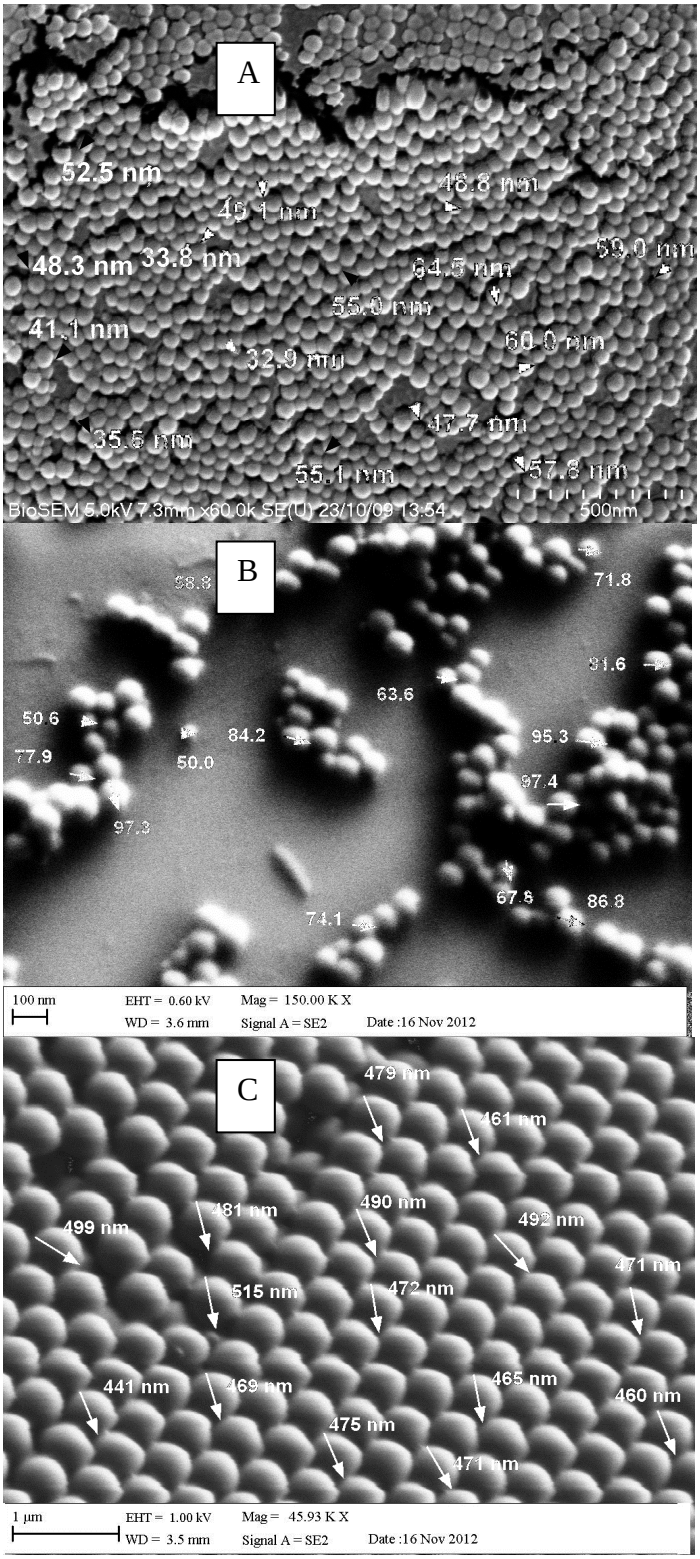

Figure S-1. SEM images of A) 52 nm, B) 81 nm and C) 465 nm PS particles

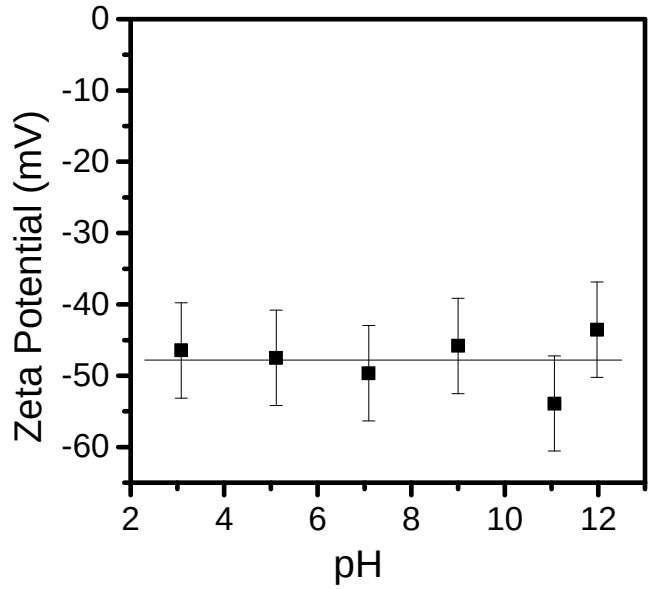

Figure S-2. Zeta potential of PS particle in background electrolyte solution of 1 mM $NaHCO_3$ and 20 mM NaCl with varying pH, line represents the mean of the zeta potential values.

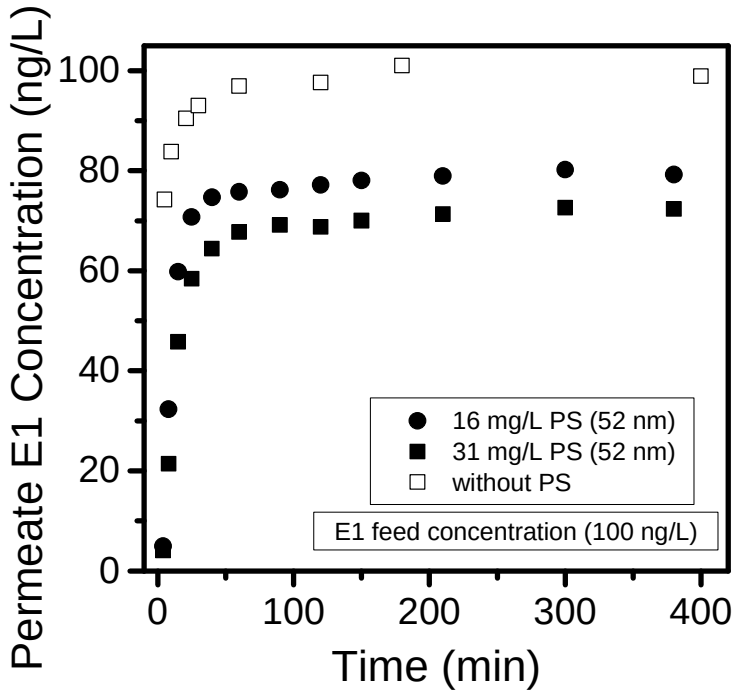

Figure S-3. The kinetics of the E1 sorption on PS nanoparticles in stirred cell: static stirred cell experiment with 52 nm PS particles, 100 ng/L E1 with 1 mM $NaHCO_3$ and 20 mM NaCl background electrolyte, pH 7

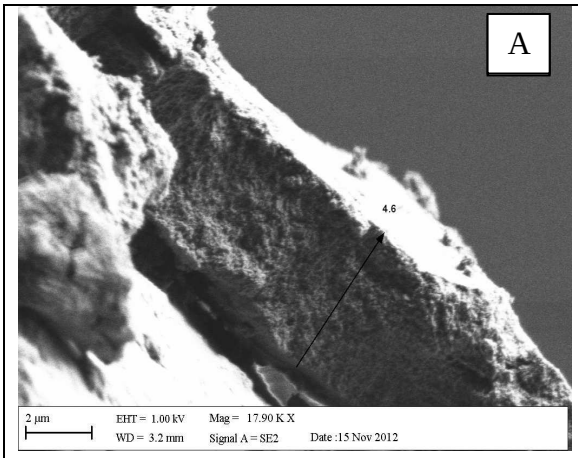
A
4.6
2 µm
EHT = 1.00 kV
WD = 3.2 mm
Mag = 17.90 K X
Signal A = SE2
Date :15 Nov 2012

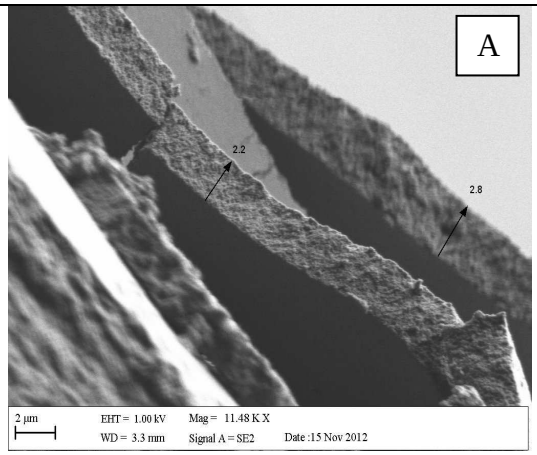
A
2.2
2.8
2 µm
EHT = 1.00 kV
WD = 3.3 mm
Mag = 11.48 K X
Signal A = SE2
Date :15 Nov 2012

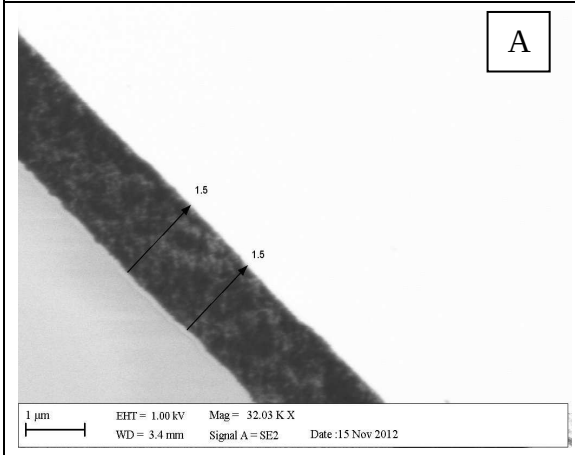
A
1.5
1.5
1 µm
EHT = 1.00 kV
WD = 3.4 mm
Mag = 32.03 K X
Signal A = SE2
Date :15 Nov 2012

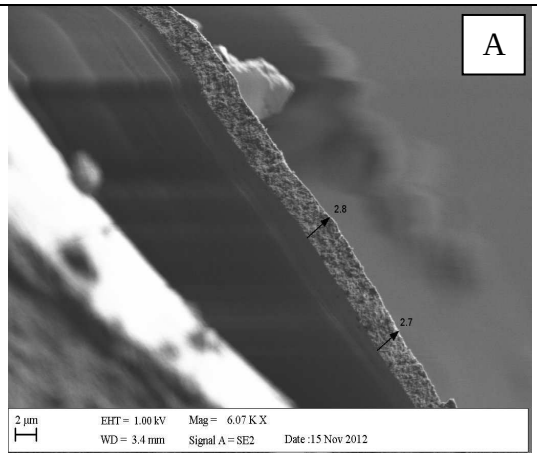
A
2.8
2.7
2 µm
EHT = 1.00 kV
WD = 3.4 mm
Mag = 6.07 K X
Signal A = SE2
Date :15 Nov 2012

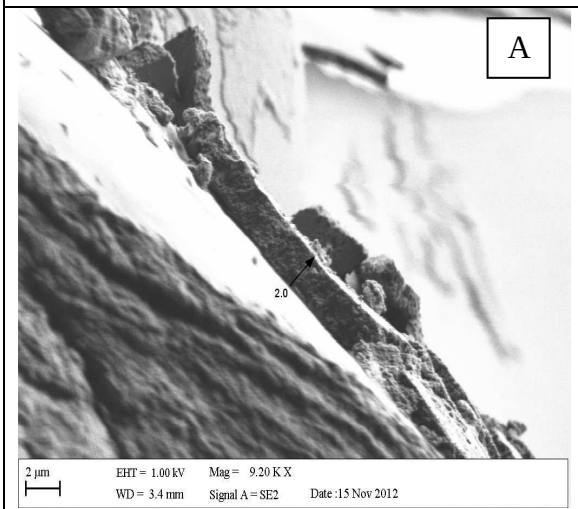
A
2.0
2 µm
EHT = 1.00 kV
WD = 3.4 mm
Mag = 9.20 K X
Signal A = SE2
Date :15 Nov 2012

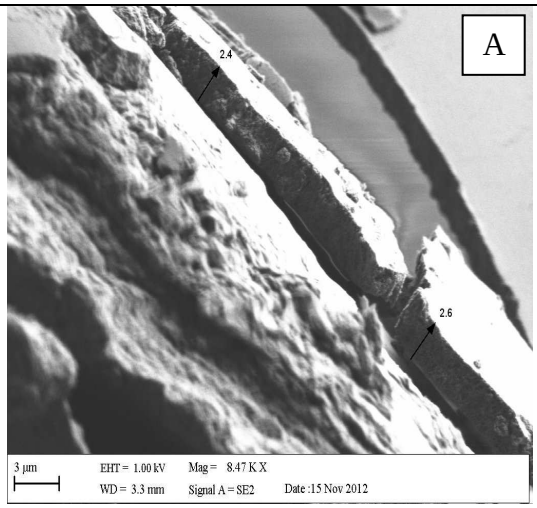
A
2.4
2.6
3 µm
EHT = 1.00 kV
WD = 3.3 mm
Mag = 8.47 K X
Signal A = SE2
Date :15 Nov 2012

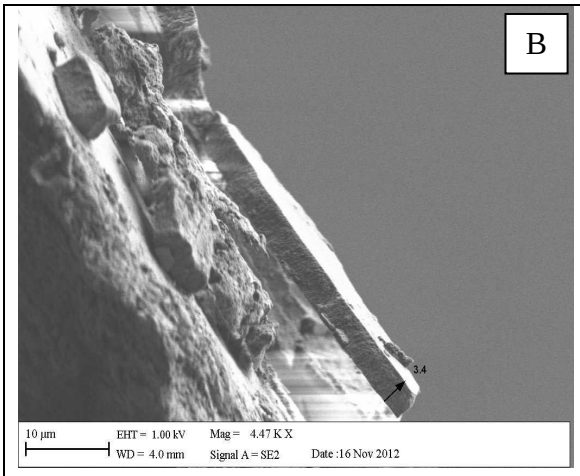
B
3.4
10 µm
EHT = 1.00 kV
WD = 4.0 mm
Mag = 4.47 K X
Signal A = SE2
Date :16 Nov 2012

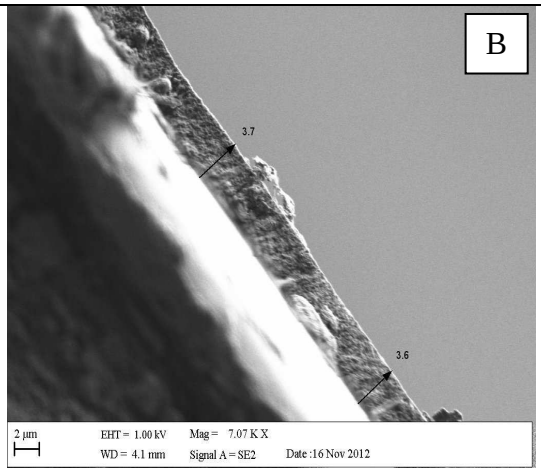
B
3.7
3.6
2 µm
EHT = 1.00 kV
WD = 4.1 mm
Mag = 7.07 K X
Signal A = SE2
Date :16 Nov 2012

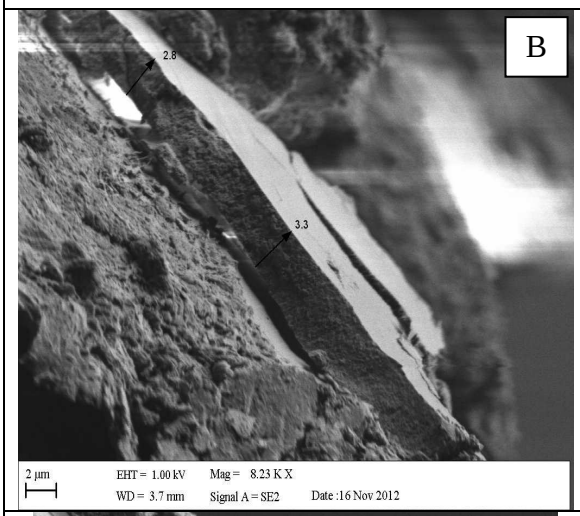
B
2.8
3.3
2 µm
EHT = 1.00 kV
WD = 3.7 mm
Mag = 8.23 K X
Signal A = SE2
Date :16 Nov 2012

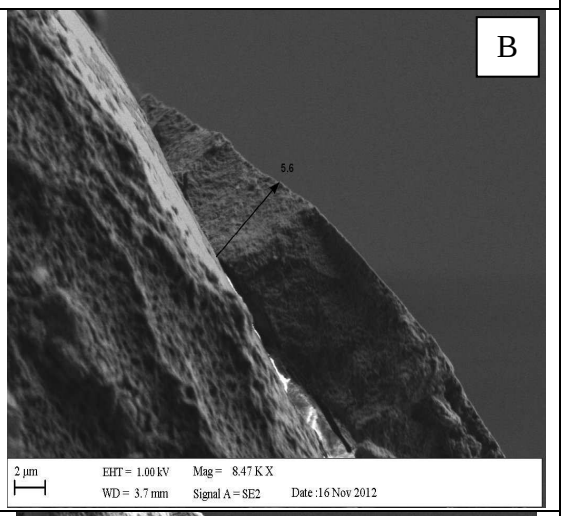
B
5.6
2 µm
EHT = 1.00 kV
WD = 3.7 mm
Mag = 8.47 K X
Signal A = SE2
Date :16 Nov 2012

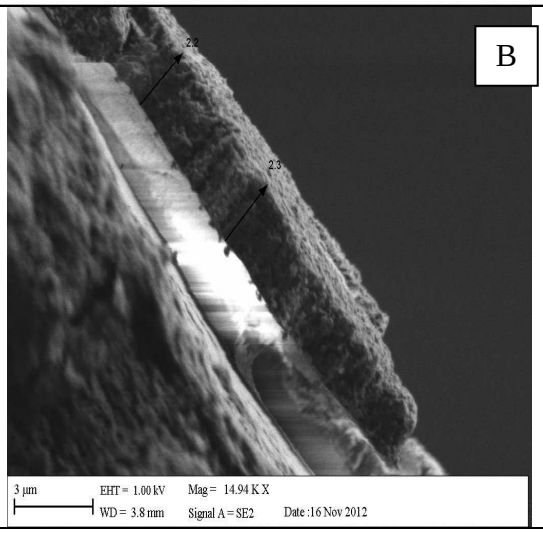
B
2.2
2.3
3 µm
EHT = 1.00 kV
WD = 3.8 mm
Mag = 14.94 K X
Signal A = SE2
Date :16 Nov 2012

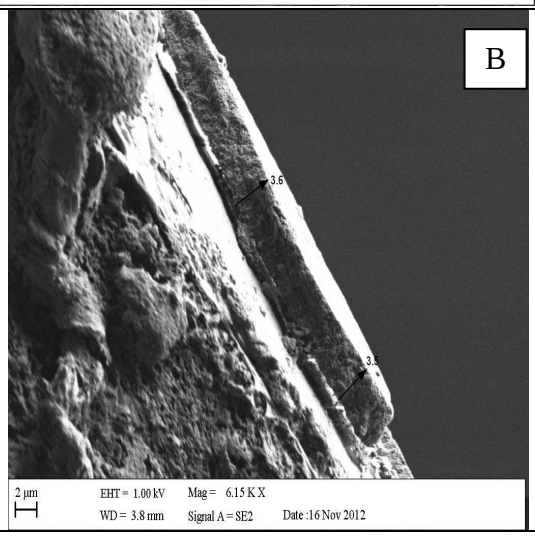
B
3.6
2 µm
EHT = 1.00 kV
WD = 3.8 mm
Mag = 6.15 K X
Signal A = SE2
Date :16 Nov 2012

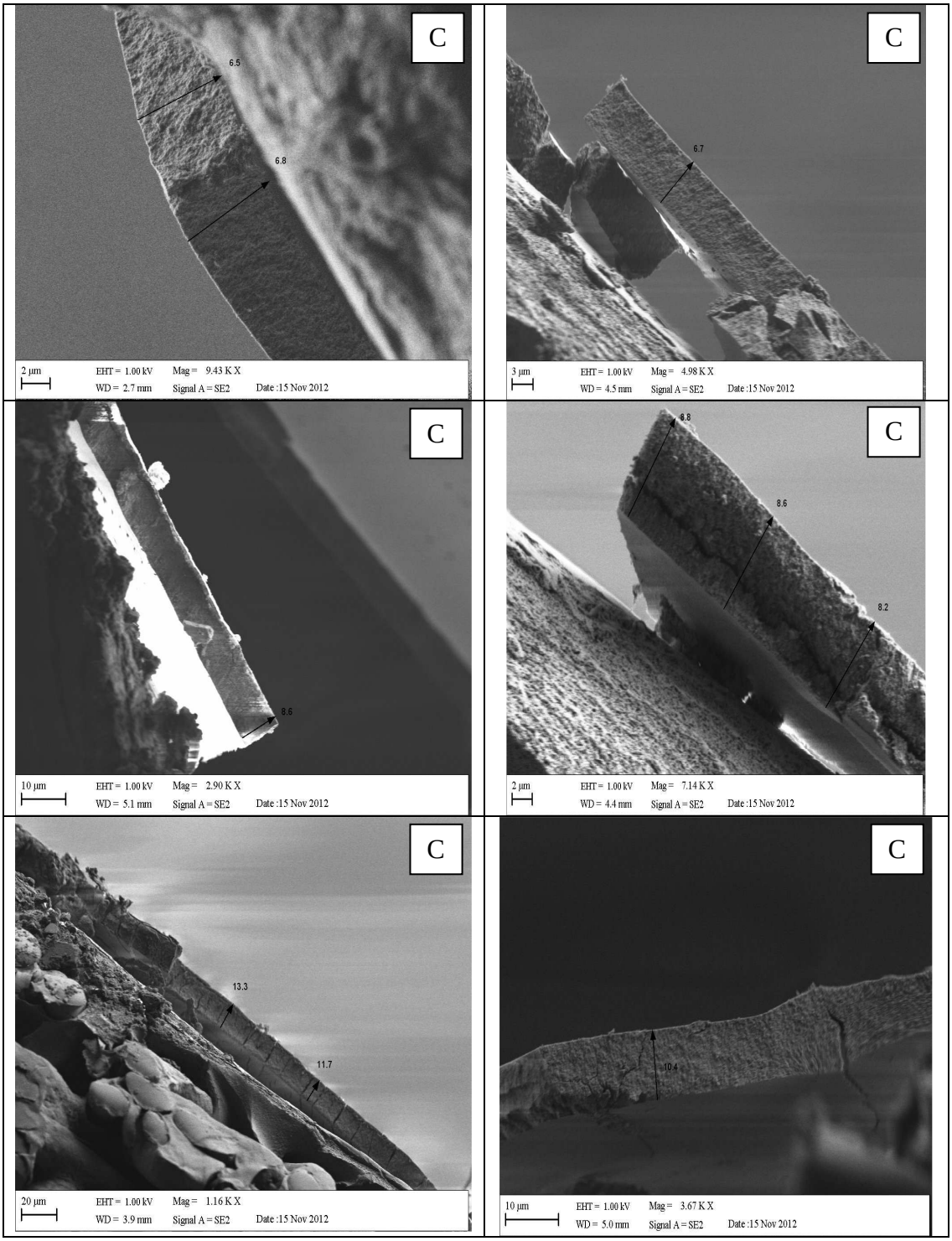

Figure S-4 Deposit thickness of 52 nm PS particles on 100 kDa UF membrane A) at 8.4 mg/L PS concentration B) at 16.8 mg/L PS concentration C) 33.5 mg/L PS concentration

Table S-1. Flux data for all filtration experiments with varying PS concentration, PS particle size and solution pH

PS Concentration	Experimental Flux (1kDa)	Experimental Flux (5kDa)	Experimental Flux (30kDa)	Experimental Flux (100kDa)
mg/L	$L/m^2.h$	$L/m^2.h$	$L/m^2.h$	$L/m^2.h$
1.7	19	48	334	374
8.4	22	42	219	277
17	20	48	179	189
34	24	43	150	94
84	20	46	90	40

PS Particle Size	Experimental Flux (30kDa)	Experimental Flux (100kDa)
nm	$L/m^2.h$	$L/m^2.h$
52	179	189
81	257	169
465	335	376
3000	331	385

pH	Experimental Flux (100kDa)
	$L/m^2.h$
5	134
7	189
11.7	142

Table S-2 Permeate E1 concentration and removal efficiency for relevant experiments

MWCO	PS feed concentration	Solution pH	PS size	E1 Feed Concentration	E1 Permeate Concentration	E1 Removal[a]
kDa	mg/L		nm	ng/L	ng/L	%
100	84	7	52	101	59	41.7
5	50	7	52	101	67	33.7
3	17	9	52	103	89	13.6

[a] data for a single experiment; for the figures average values of the repeated experiments were used.